Journal of Crystal Growth 430 (2015) 34–40

Contents lists available at ScienceDirect

Journal of Crystal Growth

journal homepage: www.elsevier.com/locate/jcrysgro

Synthesis of uniformly distributed single- and double-sided zinc oxide (ZnO) nanocombs

Ozlem Altintas Yildirim [a,b,c,*], Yuzi Liu [d], Amanda K. Petford-Long [a,e]

[a] Materials Science Division, Argonne National Laboratory, Argonne, IL 60439, USA
[b] Department of Metallurgical and Materials Engineering, Middle East Technical University, Ankara 06800, Turkey
[c] Department of Metallurgical and Materials Engineering, Selcuk University, Konya 42075, Turkey
[d] Center for Nanoscale Materials, Argonne National Laboratory, Lemont, IL 60439, USA
[e] Department of Materials Science and Engineering, Northwestern University, Evanston, IL 60208, USA

ARTICLE INFO

Article history:
Received 2 February 2015
Received in revised form
26 June 2015
Accepted 12 August 2015
Communicated by: Prof. J.M. Redwing
Available online 21 August 2015

Keywords:
A1. Nanostructures
A2. Growth from vapor
B2. Semiconducting II–VI materials

ABSTRACT

Uniformly distributed single- and double-sided zinc oxide (ZnO) nanocomb structures have been prepared by a vapor–liquid–solid technique from a mixture of ZnO nanoparticles and graphene nanoplatelets. The ZnO seed nanoparticles were synthesized via a simple precipitation method. The structure of the ZnO nanocombs could easily be controlled by tuning the carrier-gas flow rate during growth. Higher flow rate resulted in the formation of uniformly-distributed single-sided comb structures with nanonail-shaped teeth, as a result of the self-catalysis effect of the catalytically active Zn-terminated polar (0001) surface. Lower gas flow rate was favorable for production of double-sided comb structures with the two sets of teeth at an angle of ~110° to each other along the comb ribbon, which was attributed to the formation of a bicrystal nanocomb ribbon. The formation of such a double-sided structure with nanonail-shaped teeth has not previously been reported.

1. Introduction

Zinc oxide (ZnO) is an important semiconducting metal oxide with a wide direct band gap (3.37 eV) and large exciton binding energy (60 meV). Its high binding energy compared to the other prospective materials such as ZnSe (22 meV), GaN (25 meV), and ZnS (40 meV) makes ZnO a candidate material for optical applications such as laser and UV light emitting diodes [1,2]. Due to the different functional requirements in its applications, there has been strong interest in the synthesis of ZnO nanostructures with well-controlled size and shape. ZnO nanostructures with a number of special morphologies, including nanobelts [3], nanonails [4], nanowhiskers [5], and nanotetrapods [6] have been synthesized using techniques ranging from gas phase processes to solution routes. Recently, ZnO nanocomb structures have provoked great interest because of their well-defined geometry, ordered structure and potential applications in biosensors [7], solar cells [8], laser arrays [9], and nano-cantilever arrays [10]. Developing and understanding of the underlying growth mechanism of well-defined nanocomb structures is therefore of considerable significance. The growth of nanocombs with 'teeth' that are uniformly distributed on a single side, or on both sides of the comb ribbon has been reported by several groups in the literatures [11–13]. However, there remains a need to understand the growth mechanism, and thus the synthesis procedure that will results in uniformly distributed ZnO nanocombs with well-controlled shape.

In this study, we report synthesis of uniformly-aligned single- and double-sided ZnO nanocombs by oxygen-assisted carbothermal evaporation of ZnO nanoparticles synthesized through a simple room temperature precipitation. ZnO nanocombs have been fabricated over a large area on silicon wafers coated with a thin gold film. We propose possible growth mechanisms for both single- and double-sided comb-structures with nanonail-shaped teeth that can provide insights useful for large-scale production of uniformly-aligned ZnO nanocombs with potential applications in a variety of fields.

2. Experimental section

2.1. ZnO nanocomb synthesis

ZnO nanoparticles with ~20 nm particle size were prepared as seeds for the subsequent nanocomb growth. The nanoparticles were synthesized via a simple room temperature precipitation technique

* Corresponding author at: Department of Metallurgical and Materials Engineering, Selcuk University, Konya 42075, Turkey. Tel.: +90 332 223 1997; fax: +90 332 241 0635.
E-mail address: altintas@selcuk.edu.tr (O. Altintas Yildirim).

http://dx.doi.org/10.1016/j.jcrysgro.2015.08.007
0022-0248/

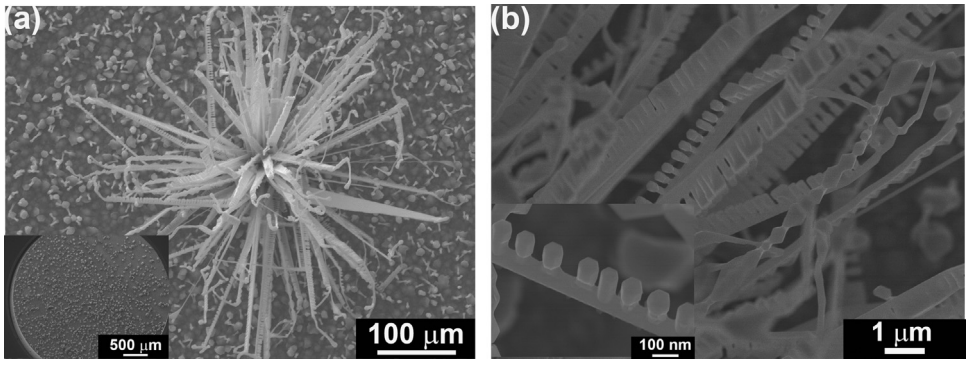

Fig. 1. (a) Low magnification SEM image of single-sided ZnO nanocomb flower prepared under a gas flow rate of 120 sccm (inset shows distribution of flowers across substrate) and (b) high magnification SEM images of nanocombs with inset showing high magnification top view of the teeth structure.

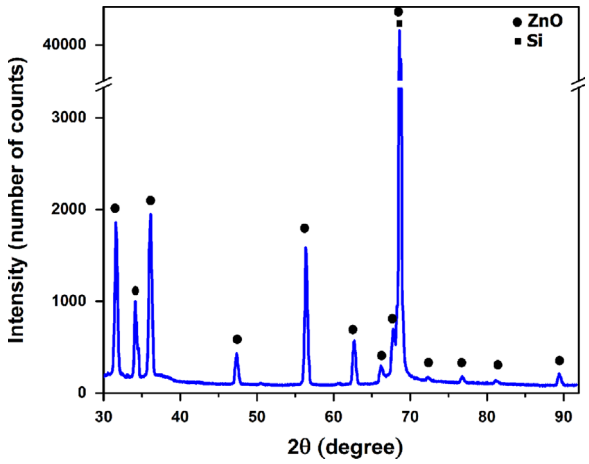

Fig. 2. XRD diffractograms of ZnO nanocombs prepared under a gas flow rate of 120 sccm.

that we have already established successfully [14]. The ZnO nanocombs were then synthesized by a vapor–liquid–solid (VLS) method. ZnO nanoparticles and graphene nanoplatelets, in a 1:1 weight ratio mixture, were ground together and placed in a quartz boat, which was inserted into a horizontal tube furnace. The graphene powder was used as a catalyst to decrease the vaporization temperature of the ZnO. P-type boron-doped prime silicon wafers were used as substrates. Prior to growth, the wafers were cleaned with an ultrasonicater in 2-proponal, acetone and DI-water, respectively. The wafer surfaces were coated with 5 nm Cr (0.036 nm/s) and 10 nm Au (0.167 nm/s) thin films using electron beam deposition. The silicon wafers were located in the furnace in a downstream position to collect the products. During the experimental process, a carrier gas mixture containing high purity Ar (98 vol%) and O_2 (2 vol%) was kept flowing into the tube furnace. Two different flow rates were used: 60 or 120 sccm (standard cubic centimeter per minute) so that the effect of gas flow rate on morphology could be explored. The tube furnace was heated to 1000 °C within 1 h and kept at the same temperature for 2 h. The furnace was then cooled to room temperature over a 3 h period. The substrates were coated with a white deposit layer.

2.2. Materials characterization

The phases of the reaction products were identified via X-ray diffraction (XRD) using Cu Kα radiation ($\lambda = 1.54056$ Å) and an x-ray source operating voltage of 40 kV. Scans were performed in the range of 28–92° at a scanning rate of 0.01°/s.

The size and morphology of the ZnO nanocombs was examined by scanning electron microscopy (SEM) and transmission electron microscopy (TEM). The SEM samples were examined without any conductive coating layer. The representative TEM samples were prepared simply by drying out an ultrasonically-dispersed aqueous suspension on holey carbon-coated copper grids.

The band structure of the nanocombs was investigated by ultraviolet-visible (UV–vis) spectroscopy and compared with that of the nanoparticle precursor. Samples were dispersed in DI-water by ultrasonification for 10 min. The background contribution was evaluated using DI-water as reference. The direct band gap energy (E_g) of the ZnO nanocombs is determined by plotting the absorption coefficient (α) versus photon energy ($h\upsilon$) and extrapolating the straight-line portion of this plot to the hυ axis. The room temperature photoluminescence (PL) spectrum measurements were measured using DI-water for the baseline correction.

3. Results

Fig. 1 shows the morphology of the VLS-grown ZnO nanostructures with a gas flow rate of 120 sccm. A flower structure with ~25 μm branches from the center is shown in Fig. 1(a). The inset low magnification SEM image shows the distribution of many flowers over the substrate surface. The high magnification SEM image (Fig. 1 (b)) shows that the branches are actually single-side nanocombs, with comb teeth length ranging from 500 nm to 1.4 μm, decreasing with distance from the flower center. The comb teeth have a hexagonal morphology (inset in Fig. 1(b)) and grow normal to the comb ribbon. The shape of each tooth can be described as a nanocone [15] or nanonail [16]. An XRD pattern from the VLS-grown nanostructures is

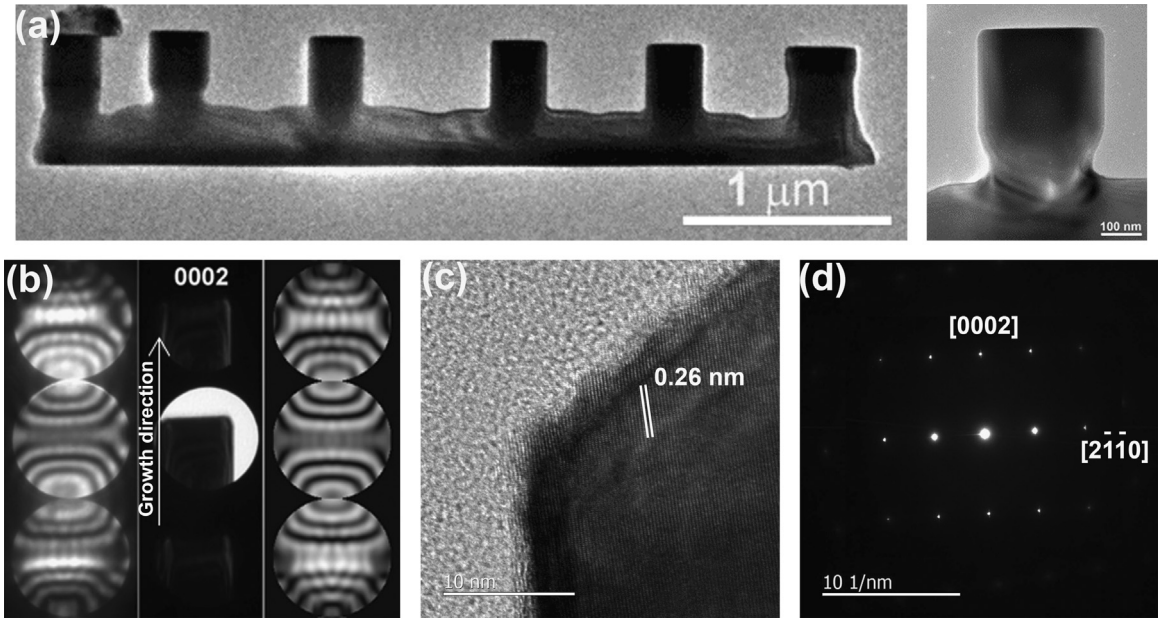

Fig. 3. (a) Low magnification TEM image of single-sided ZnO nanocombs prepared under 120 sccm gas flow rate. The inset shows an enlargement of the selected area, (b) experimental CBED pattern (left), shadow image, and simulated CBED pattern (right), (c) HRTEM image of position marked in inset to (a) and (d) corresponding SAED pattern.

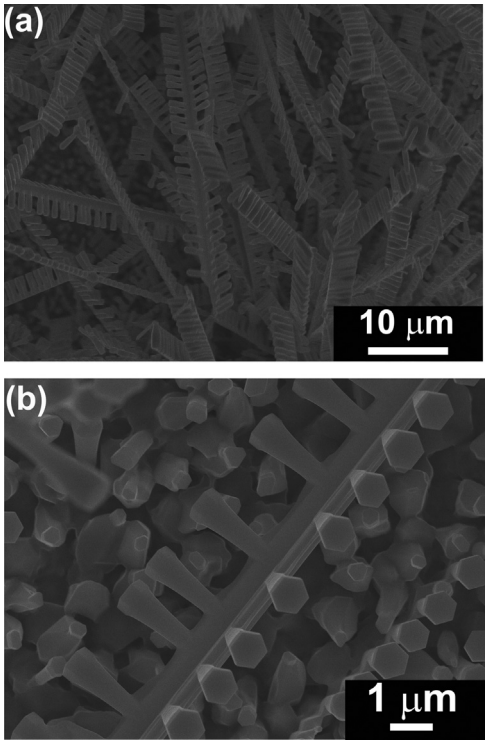

Fig. 4. (a) SEM image of single-sided ZnO nanocombs prepared under a gas flow rate of 60 sccm and (b) high magnification SEM images of asymmetric double-sided ZnO nanocombs with 110° teeth angle prepared with the same gas flow rate.

shown in Fig. 2. The nanocombs are highly crystalline ZnO with the hexagonal wurtzite structure (JCPDS Card number:36-1451). Note that the peak at an angle of $2\theta = 68.69^{\circ}$ contains counts from both the (2021) ZnO planes and the (004) planes of the Si substrate. The y-axis has therefore been modified to enable the other ZnO diffraction peaks to be clearly seen.

More detailed structural characterization of the nanocombs was carried out using TEM and HRTEM. Fig. 3(a) shows the ZnO nanocomb morphology: evenly distributed teeth can be seen along one side of the comb-ribbon. (Note that the small crystalline region on the top of the left-hand tooth is a small portion of a different nanocomb that broke off during TEM sample preparation.) The magnified image of a nanocomb tooth (inset in Fig. 3(a)) shows small indentations on the side of the comb ribbon containing the teeth, whereas the opposite surface of the ribbon is smooth and flat. The length of comb teeth is determined as ~350 nm. ZnO has a non-centrosymmetric crystal

structure, with a catalytically-active Zn-terminated polar top (0001) surface, and a catalytically-inert O-terminated polar bottom ($000\bar{1}$) surface [17,18]. To identify the polarity of the comb structure, convergent beam electron diffraction (CBED) patterns were recorded from the comb-ribbon and comb-teeth. Different intensity distributions in the (0002) and ($000\bar{2}$) disks indicate the non-central symmetric structure of ZnO, and comparison of our experimental (Fig. 3(b), left panel) CBED patterns with simulated patterns (Fig. 3(b), right panel) confirms that the nanocomb teeth grow out from the (0001) surface of the comb-ribbon. The high contrast in the discs of the CBED pattern confirms the good crystallinity of the samples, which was also confirmed by HRTEM analysis as shown in Fig. 3(c). The selected-area electron diffraction (SAED) pattern in Fig. 3 (d) shows that the growth direction of the comb-ribbon was along [$2\bar{1}\bar{1}0$]. The surfaces of the comb-ribbon parallel to the teeth and to the long axis of the ribbon are $\pm(01\bar{1}0)$ planes.

The lower gas flow rate (60 sccm) results in a different ZnO nanocomb structure, namely a mixture of double-sided and single-sided nanocombs, as seen in Fig. 4. The low magnification SEM image in Fig. 4(a) shows that the comb-ribbon length is ~45–50 μm, which is almost twice that of the nanocombs produced under high gas flow. Fig. 4(b) shows a high magnification SEM image of a typical double-sided comb structure. The double-sided nanocomb teeth show a similar morphology to the single-sided nanocomb teeth, growing at regular intervals along the nanocomb ribbon with a nanonail shape. However the double-sided ZnO comb ribbons show a different morphology to those of the single-sided combs, with a ribbon cross-section shaped like an open 'L'. The two sets of comb teeth then grow out from each end surface of the 'L', at an angle of ~110° to each other along the ZnO nanocomb ribbon. The hexagonal end-shape of the tips of the comb-teeth suggests that they preferentially grow along a [0001] direction, which was confirmed by SAED analysis (not shown here).

Fig. 5(a) shows a TEM image of the single-sided comb structure produced under the lower gas flow rate. The length of the comb teeth in the case of lower gas flow rate (~2 μm) is considerably larger for the combs grown under higher gas flow rate. Fig. 5(b) is a dark field TEM image of the same comb structure seen in Fig. 5(a). The contrast differences indicate that there is a thickness difference between the region of comb-ribbon and teeth and between the comb–teeth themselves.

3.1. Optical behavior

Fig. 6 shows UV–vis absorption spectra from the ZnO precursor nanoparticles and single-sided nanocombs. The absorption band edge for the nanocomb structure shows a red shift to higher wavelength (341.5 nm) than for the ZnO nanoparticle precursors (336.2 nm). The plots used to determine the direct band gap (E_g) are inset. E_g is 3.38 eV for the precursor nanoparticles and it decreases to 3.29 eV for the nanocombs. Fig. 6(b) shows a comparison between the photoluminescence (PL) spectra for the precursor nanoparticles and the nanocombs grown with a 120 sccm gas flow rate. In addition to the second order band-edge emission at 1.67 eV, the shape of the peak at ~3.25 eV becomes more complicated for the nanocombs, showing a double peak with emission bands in the violet (3.13 eV) and UV (3.38 eV).

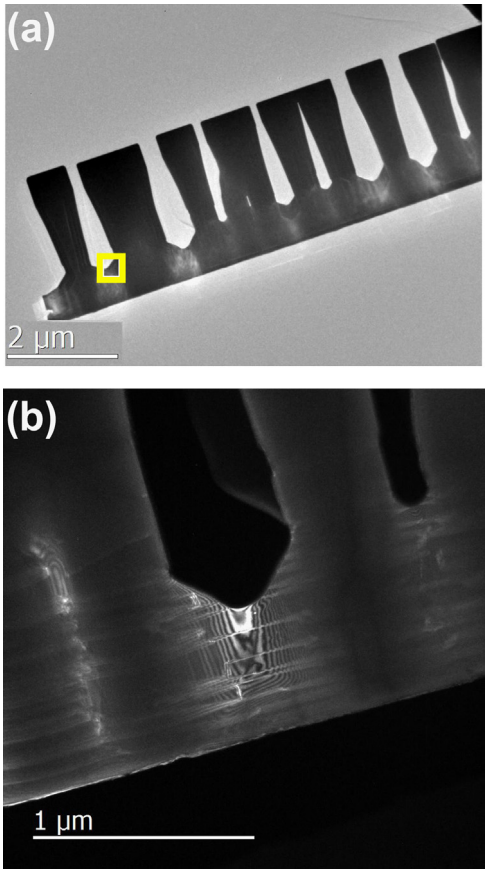

Fig. 5. (a) Low magnification TEM image of single-sided nanocomb prepared under a gas flow rate of 60 sccm, (b) dark-field TEM image of area outlined in (a).

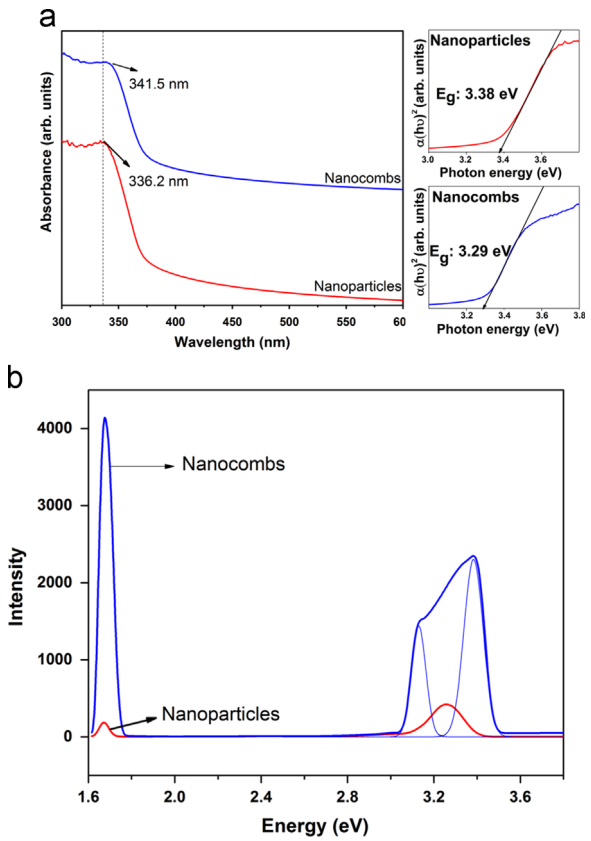

Fig. 6. (a) UV–vis spectra and (b) PL spectra for ZnO nanoparticles and nanocombs prepared under a gas flow rate of 120 sccm. Band edge locations are indicated in (a). The insets show plots of $(\alpha h\upsilon)^2$ as a function of photon energy with values of E_g for both nanoparticles and nanocombs.

4. Discussion

4.1. Nanocomb growth model

4.1.1. Single-sided nanocombs

We proposed that the growth kinetics of the nanocombs are the result of rapid crystallization at large supersaturation, with growth proceeding via a VLS process. At the reaction temperature (1000 °C), ZnO nanoparticles are evaporated to form zinc vapor, which is transported by the Ar carrier gas, consumed by the introduced oxygen, and finally deposited on the catalyst Au liquid droplets on the silicon substrate in the form of ZnO. During the nanocomb growth, the dimension and morphology of the Au catalyst layer plays an important role in determining the morphology of the ZnO nanostructures that form. Xu et al. reported that a comb-structure can be obtained by the usage of 1-D Au nanowires and 2-D Au films; however, nanorod arrays can be achieved when 0-D Au nanodots are used [19]. In our case, we believe that the thin Au film balls up at high temperature to reduce its surface energy, forming liquid Au islands that enable the flower structures to grow with many branches coming out from the flower center. EDX analysis (included in Supplementary material) of the comb ribbons and teeth showed a reduction in Au content along the comb-ribbon, indicating a lowering of Au diffusion away from the flower center. This reduction in Au content will self-limit the length of comb-ribbon that can form and also leads to a reduction in tooth length along the comb ribbon. Note that Au was also observed at the tips of the comb teeth.

Once the ZnO nanocomb-ribbons reach a certain length via the continuous evaporation of zinc, comb-teeth starts to grow. Several different growth directions have been reported for ZnO comb-ribbons including [0001] [20], $[11\bar{2}0]$ [19,21], $\{10\bar{1}0\}$ [15,22,23], and $[2\bar{1}\bar{1}0]$ [8,12,24,25]. The single-sided nanocombs discussed here, which form under a gas flow of 120 sccm, have a growth direction of $[2\bar{1}\bar{1}0]$ along the ribbon. The hexagonal end-shape of the comb teeth results from their [0001] growth direction, which was confirmed as shown in Fig. 3(b).

The formation mechanism of single-sided nanocombs with comb teeth growing along the [0001] direction has been ascribed to the self-catalysis effect of the polar Zn-terminated (0001) surface [10]: as a result of the different chemical activity of the polar surfaces, the (0001)-Zn and $(000\bar{1})$-O terminated surfaces exhibit different growth behaviors. The chemically-active Zn-terminated surface provides a backdrop to initiate local enrichment of Zn on the surface of the comb-ribbon. However, as has been pointed out by Comjani et al. [26] this model does not account for the regular spacing of the comb teeth, and they have proposed a further model that additionally takes into account the piezoelectric charge across the nanocomb. According to their theory, the polar surfaces introduce strain and electric potential in the first atomic layers at the crystal surfaces, leading to charge rearrangement and to non-homogeneous Zn^{2+} and O^{2-} ion densities on the polar (0001) and $(000\bar{1})$ surfaces, respectively. These spatially-distributed regions of higher positive charge on the (0001)-Zn surface act as catalysts for tooth growth. Although the O^{2-} ion density on the $(000\bar{1})$ surface is also non-homogeneous, teeth growth does not occur due to its catalytically inactive nature. Tooth growth has the effect of reducing the (0001) surface energy, which is further reduced by thinning down the areas between the teeth (Fig. 5(b)). The formation of longer single-sided comb-ribbons and comb–teeth under lower gas flow rate is due to the fact that both ribbon and teeth are exposed to more ion bombardment and thus a higher axial growth rate.

4.1.2. Double-sided nanocombs

A number of authors have reported the growth of double-sided nanocombs under certain growth conditions. For example Zhang et al. reported that double-sided ZnO nanocombs can form instead of single-sided ones by controlling the oxygen and zinc partials pressures inside the reaction chamber [12]. They found that lower oxygen partial pressure and higher zinc vapor pressure favors the growth of double-side ZnO nanocomb structures, and this is consistent with our observation of the formation of double-sided nanocombs when the carrier gas flow rate is reduced from 120 sccm to 60 sccm. The lower flow rate allows for a higher partial pressure of Zn vapor within the chamber, increasing the probability of a reaction between zinc and oxygen and thus enabling the formation of the double-sided combs. However the nanocombs reported by Zhang et *al.* have flat nanocomb ribbons with teeth projecting from the two opposite surfaces. The geometry that we observe is different, with the nanocomb ribbon cross-section being shaped like an open 'L', with nanonail-shaped teeth growing from the ends of both branches of the 'L'. Huang et al. [27] and Phan et al. [28] proposed that such structures could form as the result of the growth of bicrystalline nanocomb ribbons that have a twin parallel to the long axis of the ribbon. In the observations by Huang and by Phan, the growth direction was along $[10\bar{1}0]$ and the twins formed on a $\{10\bar{1}3\}$ plane, resulting in two surfaces along the comb ribbon that are at $\sim 120^\circ$ to each other and are both chemically-active (0001) surfaces. Teeth grow out from each of these surfaces resulting in double-sided nanocombs.

In our case the growth orientation for the double-sided nanocombs, along the comb ribbon, is $[11\bar{2}0]$ with the two sets of teeth being at an angle of $\sim 110^\circ$ to each other, and both with a growth direction along [0001]. This growth mode can be explained by a model reported by Lao et al. [25] in which four tetrahedra, each enclosed by one {0001} face and three $\{11\bar{2}2\}$ faces, are combined together to form a square pyramid whose triangular faces are alternately (0001) and $(000\bar{1})$ planes. We propose that the twin plane that forms between the two sets of teeth is a $\{10\bar{1}3\}$ plane, as has also been reported for nanostructures composed of the wurtzite phase of ZnS [29].

It is interesting to note that the papers discussed above report the formation of feather-shaped double-sided nanocombs for which the teeth are flat or needle-shaped: to the best of our knowledge we are the first to report the synthesis of bicrystal twinned double-sided nanocombs with nanonail-shaped teeth, which could have formed via the mechanism reported by Yan et al. [30].

4.2. Optical behavior

The absorption band edge of single-sided nanocombs (341.5 nm) shows a red shift compared to values that of precursor nanoparticles (336.2 nm). According to previous reports, absorption edges and thus E_g values of ZnO nanostructures mainly depend on size, morphology, defect state and dopant content [31–34]. The effects of quantum confinement and impurity atoms can be eliminated for the contraction of the band gap energy of single-sided nanocombs due to their large size, and pure structure, respectively. Therefore, this reduction may be explained by either the morphology change from the spherical nanoparticles to single-sided comb structure [35–37] or the presence of the defect states such as oxygen vacancy and zinc interstitial [38,39]. At this moment, the role of defect states is considered to be most important for the band gap narrowing due to strong exchange interaction between valance band electrons and defect state electrons.

The large peak that appears at 1.67 eV in the PL spectra for the ZnO nanocombs prepared with 120 sccm gas flow rate is attributed to second order diffraction of UV emission [40–42]. This peak appears only in the nanostructures with a strong UV emission peak and shows higher crystallite structure. The shape of the peak between $\sim$3.0–3.4 eV shows that it is a combination of two different Gaussian peaks with violet and UV emissions. The violet emission (3.13 eV) is associated with exciton recombination between the electrons at the shallow donor zinc interstitial defect level (Zn_i) and holes in the valance band of ZnO [43]. The absence of green emission (a broad peak between 1.6–2.8 eV) associated with oxygen vacancies [44] show that the single-sided ZnO nanocombs are synthesized in an environment of higher partial pressure of oxygen. This is consistent with the higher gas flow rate used to form the single-sided nanocombs: the zinc vapor formed in the reaction chamber is transported faster by the Ar carrier gas, resulting in a reduced partial pressure of zinc. The Gaussian-fitted UV-emission peak position is blue shifted towards higher energies (3.38 eV) compared with that of the bulk ZnO. The blue-shift in the UV-emission of the nanocombs can be explained by surface resonance effects [45], interface effects [46] and localized energy states [47], which can affect the electronic and optical properties and result in a shift of the UV emission peak position. Indeed the position of the UV-emission peak has been shown to exhibit distinctive values for the different nanostructures: 3.29 eV for nanorods [48], 3.21 eV for nanosheets [49], and 3.32 eV for ultrathin nanobelts [50]. We believe that defect generation on the surface of the nanocombs (Zn_i) has an influence on the spectral shift in the UV-emission. A similar observation was also reported by Rao et al. [51]. They found that the presence of Zn_i and zinc vacancy (V_{Zn}) defect states have an important role in the blue-shift of UV emission in ZnO.

5. Conclusions

Single- and double-sided ZnO nanocomb-structures with nanonail-shaped teeth were grown on silicon wafers through a VLS method, using a powder mixture of graphene and ZnO nanoparticles as source material and Au as the catalyst. The morphology of the comb-structures is strongly affected by the carrier gas flow rate during the growth of the nanocombs with lower gas rate resulting in high zinc vapor pressure inside the reaction chamber and the formation of double-sided nanocombs. Our results support a self-catalytic effect leading to comb-tooth growth on the chemically-active Zn-terminated polar (0001) surface of the nanocomb ribbon, and further invoke the influence of a piezoelectric effect to explain the regular periodic tooth formation. The synthesis of asymmetric double-sided nanocombs with two sets of teeth at $\sim 110^\circ$ to each other along the nanocomb ribbon is explained by the formation of bicrystalline nanocomb ribbons with two chemically-active (0001) surfaces. We believe this to be the first report of asymmetric double-sided nanocombs with nanonail-shaped teeth. All nanocombs presented here are highly oriented and form part of uniformly distributed ZnO hierarchical structures with promise for applications in some special fields.

Acknowledgments

OAY thanks The Scientific and Technological Research Council of Turkey (TUBITAK), Turkey for support by the National Scholarship Program for Ph.D. students and also by the METU-ÖYP Program. AKPL acknowledges support from the U.S. Department of Energy, U. S. Office of Science, U.S. Basic Energy Sciences, Materials Sciences and Engineering Division at at Argonne National Laboratory. Use of Center for Nanoscale Materials was supported by the U.S. Department of Energy, Office of Science, Office of Basic Energy Sciences, under Contract no. DE-AC02-06CH11357.

Appendix A. Supporting information

Supplementary data associated with this article can be found in the online version at http://dx.doi.org/10.1016/j.jcrysgro.2015.08.007.

References

[1] L. Znaidi, G.J.A.A. Soler Illia, S. Benyahia, C. Sanchez, A.V. Kanaev, Oriented ZnO thin films synthesis by sol–gel process for laser application, Thin Solid Films 428 (2003) 257–262.
[2] Y. Ryu, T.-S. Lee, J.A. Lubguban, H.W. White, B.-J. Kim, Y.-S. Park, C.-J. Youn, Next generation of oxide photonic devices: ZnO-based ultraviolet light emitting diodes, Appl. Phys. Lett. 88 (2006) 1–3.
[3] X.D. Bai, P.X. Gao, Z.L. Wang, E.G. Wang, Dual-mode mechanical resonance of individual ZnO nanobelts, Appl. Phys. Lett. 82 (2003) 4806–4808.
[4] D. Fan, R. Zhang, X. Wang, Synthesis and optical property of ZnO nanonail arrays with controllable morphology, Phys. E: Low-dimens. Syst. Nanostruct. 42 (2010) 2081–2085.
[5] X.-Y. Ma, W.-D. Zhang, Effects of flower-like ZnO nanowhiskers on the mechanical, thermal and antibacterial properties of waterborne polyurethane, Polym. Degrad. Stab. 94 (2009) 1103–1109.
[6] H. Yan, R. He, J. Pham, P. Yang, Morphogenesis of one-dimensional ZnO nano- and microcrystals, Adv. Mater. 15 (2003) 402–405.
[7] J.X. Wang, X.W. Sun, A. Wei, Y. Lei, X.P. Cai, C.M. Li, Z.L. Dong, Zinc oxide nanocomb biosensor for glucose detection, Appl. Phys. Lett. 88 (2006) 233106.
[8] A. Umar, Growth of comb-like ZnO nanostructures for dye-sensitized solar cells applications, Nanoscale Res. Lett. 4 (2009) 1004–1008.
[9] H. Yan, R. He, J. Johnson, M. Law, R.J. Saykally, P. Yang, Dendritic nanowire ultraviolet laser array, J. Am. Chem. Soc. 125 (2003) 4728–4729.
[10] Z.L. Wang, X.Y. Kong, J.M. Zuo, Induced growth of asymmetric nanocantilever arrays on polar surfaces, Phys. Rev. Lett. 91 (2003) 185502.
[11] U. Manzoor, D.K. Kim, Synthesis and enhancement of ultraviolet emission by post-thermal treatment of unique zinc oxide comb-shaped dendritic nanostructures, Scr. Mater. 54 (2006) 807–811.
[12] Y.H. Zhang, X.B. Song, J. Zheng, H.H. Liu, X.G. Li, L.P. You, Symmetric and asymmetric growth of ZnO hierarchical nanostructures: nanocombs and their optical properties, Nanotechnology 17 (2006) 1916–1921.
[13] C.S. Lao, P.X. Gao, R.S. Yang, Y. Zhang, Y. Dai, Z.L. Wang, Formation of double-side teethed nanocombs of ZnO and self-catalysis of Zn-terminated polar surface, Chem. Phys. Lett. 417 (2006) 358–362.
[14] O.A. Yildirim, C. Durucan, Effect of precipitation temperature and organic additives on size and morphology of ZnO nanoparticles, J. Mater. Res. 27 (2012) 1452–1461.
[15] R.F. Zhuo, H.T. Feng, Q. Liang, J.Z. Liu, J.T. Chen, D. Yan, J.J. Feng, H.J. Li, S. Cheng, B.S. Geng, X.Y. Xu, J. Wang, Z.G. Wu, P.X. Yan, G.H. Yue, Morphology-controlled synthesis, growth mechanism, optical and microwave absorption properties of ZnO nanocombs, J. Phys. D: Appl. Phys. 41 (2008).
[16] G.Z. Shen, Y. Bando, B.D. Liu, D. Golberg, C.J. Lee, Characterization and field-emission properties of vertically aligned ZnO nanonails and nanopencils fabricated by a modified thermal-evaporation process, Adv. Funct. Mater. 16 (2006) 410–416.
[17] P.X. Gao, Z.L. Wang, Substrate atomic-termination-induced anisotropic growth of ZnO nanowires/nanorods by the VLS process, J. Phys. Chem. B 108 (2004) 7534–7537.
[18] Z.L. Wang, Zinc oxide nanostructures: growth, properties and applications, J. Phys.: Condens. Mater. 16 (2004) R829–R858.
[19] X. Xu, M. Wu, M. Asoro, P.J. Ferreira, D.L. Fan, One-step hydrothermal synthesis of comb-like ZnO nanostructures, Cryst. Growth Des. 12 (2012) 4829–4833.
[20] Y.H. Huang, Y. Zhang, J. He, Y. Dai, Y.S. Gu, Z. Ji, C. Zhou, Fabrication and characterization of ZnO comb-like nanostructures, Ceram. Int. 32 (2006) 561–566.
[21] Y.Q. Chen, J. Jiang, Z.Y. He, Y. Su, D. Cai, L. Chen, Growth mechanism and characterization of ZnO microbelts and self-assembled, Mater. Lett. 59 (2005) 3280–3283.
[22] S. Yin, Y.Q. Chen, Y. Su, Q.T. Zhou, Preparation and photoluminescence of ZnO comb-like structure and nanorod arrays, Chin. J. Chem. Phys. 20 (2007) 308–314.
[23] Y.H. Leung, A.B. Djurisic, J. Gao, M.H. Xie, Z.F. Wei, S.J. Xu, W.K. Chan, Zinc oxide ribbon and comb structures: synthesis and optical properties, Chem. Phys. Lett. 394 (2004) 452–457.
[24] Y.H. Zhang, J. Liu, T. Liu, L.P. You, X.G. Li, Supersaturation-controlled synthesis of two types of single-sided ZnO comb-like nanostructures by thermal evaporation at low temperature, J. Cryst. Growth 285 (2005) 541–548.
[25] C.S. Lao, P.M. Gao, R. Sen Yang, Y. Zhang, Y. Dai, Z.L. Wang, Formation of double-side teethed nanocombs of ZnO and self-catalysis of Zn-terminated polar surface, Chem. Phys. Lett. 417 (2006) 358–362.
[26] F.F. Comjani, U. Willer, S. Kontermann, W. Schade, Modelling the growth of ZnO nanocombs based on the piezoelectric effect, AIP Adv. 3 (2013).
[27] Y.H. Huang, Y. Zhang, X.D. Bai, J. He, J. Liu, X.M. Zhang, Bicrystalline zinc oxide nanocombs, J. Nanosci. Nanotechnol. 6 (2006) 2566–2570.
[28] T.L. Phan, Y.K. Sun, R. Vincent, Structural characterization of CVD-grown ZnO nanocombs, J. Korean Phys. Soc. 59 (2011) 60–64.
[29] D. Moore, Z.L. Wang, Growth of anisotropic one-dimensional ZnS nanostructures, J. Mater. Chem. 16 (2006) 3898–3905.
[30] Y.G. Yan, L.X. Zhou, Z.D. Han, Y. Zhang, Growth analysis of hierarchical ZnO nanorod array with changed diameter from the aspect of supersaturation ratio, J. Phys. Chem. C 114 (2010) 3932–3936.
[31] K.-F. Lin, H.-M. Cheng, H.-C. Hsu, L.-J. Lin, W.-F. Hsieh, Band gap variation of size-controlled ZnO quantum dots synthesized by sol–gel method, Chem. Phys. Lett. 409 (2005) 208–211.
[32] R. Rusdi, A.A. Rahman, N.S. Mohamed, N. Kamarudin, N. Kamarulzaman, Preparation and band gap energies of ZnO nanotubes, nanorods and spherical nanostructures, Powder Technol. 210 (2011) 18–22.
[33] D. Verma, A.K. Kole, P. Kumbhakar, Red shift of the band-edge photoluminescence emission and effects of annealing and capping agent on structural and optical properties of ZnO nanoparticles, J. Alloy. Compd. 625 (2015) 122–130.
[34] Ö.A. Yıldırım, H.E. Unalan, C. Durucan, Highly efficient room temperature synthesis of silver-doped zinc oxide (ZnO:Ag) nanoparticles: structural, optical, and photocatalytic properties, J. Am. Ceram. Soc. 96 (2013) 766–773.
[35] J.H. Zhang, H.Y. Liu, Z.L. Wang, N.B. Ming, Z.R. Li, A.S. Biris, Polyvinylpyrrolidone-directed crystallization of ZnO with tunable morphology and bandgap, Adv. Funct. Mater. 17 (2007) 3897–3905.
[36] X.C. Li, G.H. He, G.K. Xiao, H.J. Liu, M. Wang, Synthesis and morphology control of ZnO nanostructures in microemulsions, J. Colloid Interface Sci. 333 (2009) 465–473.
[37] N. Samaele, P. Amornpitoksuk, S. Suwanboon, Effect of pH on the morphology and optical properties of modified ZnO particles by SDS via a precipitation method, Powder Technol. 203 (2010) 243–247.
[38] F. Kayaci, S. Vempati, I. Donmez, N. Biyikli, T. Uyar, Role of zinc interstitials and oxygen vacancies of ZnO in photocatalysis: a bottom-up approach to control defect density, Nanoscale 6 (2014) 10224–10234.
[39] P. Erhart, K. Albe, A. Klein, First-principles study of intrinsic point defects in ZnO: role of band structure, volume relaxation, and finite-size effects, Phys. Rev. B 73 (2006) 205203.
[40] Y.G. Wang, S.P. Lau, H.W. Lee, S.F. Yu, B.K. Tay, X.H. Zhang, H.H. Hng, Photoluminescence study of ZnO films prepared by thermal oxidation of Zn metallic films in air, J. Appl. Phys. 94 (2003) 354–358.
[41] J.G. Lv, C.L. Liu, W.B. Gong, Z.F. Zi, X.S. Chen, K. Huang, T. Wang, G. He, S.W. Shi, X.P. Song, Z.Q. Sun, Temperature-dependent shifts of near band-edge emission and their second-order diffraction for ZnO nanorods, Opt. Mater. 34 (2012) 1917–1920.
[42] W.W. Li, W.L. Yu, Y.J. Jiang, C.B. Jing, J.Y. Zhu, M. Zhu, Z.G. Hu, X.D. Tang, J. H. Chu, Structure, optical, and room-temperature ferromagnetic properties of pure and transition-metal-(Cr, Mn, and Ni)-doped ZnO nanocrystalline films grown by the sol gel method, J. Phys. Chem. C 114 (2010) 11951–11957.
[43] B.Q. Cao, W.P. Cai, H.B. Zeng, Temperature-dependent shifts of three emission bands for ZnO nanoneedle arrays, Appl. Phys. Lett. 88 (2006).
[44] H.S. Kang, J.S. Kang, J.W. Kim, S.Y. Lee, Annealing effect on the property of ultraviolet and green emissions of ZnO thin films, J. Appl. Phys. 95 (2004) 1246–1250.
[45] C.-W. Chen, K.-H. Chen, C.-H. Shen, A. Ganguly, L.-C. Chen, J.-J. Wu, H.-I. Wen, W.-F. Pong, Anomalous blueshift in emission spectra of ZnO nanorods with sizes beyond quantum confinement regime, Appl. Phys. Lett. 88 (2006).
[46] X.-M. Zhang, M.-Y. Lu, Y. Zhang, L.-J. Chen, Z.L. Wang, Fabrication of a high-brightness blue-light-emitting diode Using a ZnO-nanowire array grown on p-GaN Thin Film, Adv. Mater. 21 (2009) 2767–2770.
[47] T. Mukai, M. Yamada, S. Nakamura, Current and temperature dependences of electroluminescence of InGaN-based UV/blue/green light-emitting diodes, Jpn. J. Appl. Phys. Part 2-Lett. 37 (1998) L1358–L1361.
[48] W.I. Park, D.H. Kim, S.-W. Jung, G.-C. Yi, Metalorganic vapor-phase epitaxial growth of vertically well-aligned ZnO nanorods, Appl. Phys. Lett. 80 (2002) 4232–4234.
[49] S. Kar, A. Dev, S. Chaudhuri, Simple solvothermal route to synthesize ZnO nanosheets, nanonails, and well-aligned nanorod arrays, J. Phys. Chem. B 110 (2006) 17848–17853.
[50] X.D. Wang, Y. Ding, C.J. Summers, Z.L. Wang, Large-scale synthesis of six-nanometer-wide ZnO nanobelts, J. Phys. Chem. B 108 (2004) 8773–8777.
[51] T. Prasada Rao, G.K. Goswami, K.K. Nanda, Detailed understanding of the excitation-intensity dependent photoluminescence of ZnO materials: role of defects, J. Appl. Phys. 115 (2014) 213513.